Cytosolic aggregates perturb the degradation of nontranslocated secretory and membrane proteins

Oishee Chakrabarti*, Neena S. Rane, and Ramanujan S. Hegde
Cell Biology and Metabolism Program, Eunice Kennedy Shriver National Institute of Child Health and Human Development, National Institutes of Health, Bethesda, MD 20892

ABSTRACT **A wide range of diseases are associated with the accumulation of cytosolic protein aggregates. The effects of these aggregates on various aspects of normal cellular protein homeostasis remain to be determined. Here we find that cytosolic aggregates, without necessarily disrupting proteasome function, can markedly delay the normally rapid degradation of nontranslocated secretory and membrane protein precursors. In the case of mammalian prion protein (PrP), the nontranslocated fraction is recruited into preexisting aggregates before its triage for degradation. This recruitment permits the growth and persistence of cytosolic PrP aggregates, explaining their apparent "self-conversion" seen in earlier studies of transient proteasome inhibition. For other proteins, the aggregate-mediated delay in precursor degradation led to aggregation and/or soluble residence in the cytosol, often causing aberrant cellular morphology. Remarkably, improving signal sequence efficiency mitigated these effects of aggregates. These observations identify a previously unappreciated consequence of cytosolic aggregates for nontranslocated secretory and membrane proteins, a minor but potentially disruptive population the rapid disposal of which is critical to maintaining cellular homeostasis.**

Monitoring Editor
Thomas Sommer
Max Delbrück Center for Molecular Medicine

Received: Jul 27, 2010
Revised: Feb 23, 2011
Accepted: Mar 7, 2011

INTRODUCTION

Protein aggregation is a common feature in various diseases (Selkoe, 2003; Rubinsztein 2006; Soto *et al.*, 2006; Aguzzi and Rajendran, 2009). Pathologic cellular aggregates are generally composed of misfolded or incompletely folded proteins. In many diseases, a single protein species (typically a mutant version of a normal protein) is thought to initiate aggregation and form its major component. These aggregates are often sequestered in discrete structures variously termed inclusion bodies, aggresomes, various disease-specific morphological structures (e.g., Lewy bodies), and other more recently described cytological structures (Kopito, 2000; Kaganovich *et al.*, 2008). Because of their conspicuous association with disease, considerable work has been done to investigate aggregate structure (especially amyloid), aggregate formation, and aggregate clearance. By contrast, delineation of the specific cellular consequences of aggregates has only recently received significant attention.

Typically, protein aggregation diseases are dominant "gain-of-function" disorders. Hence it is not necessarily the loss of the aggregate-prone protein to the aggregate that leads to cellular phenotypes, but the gain of a new functional property of the protein and/or aggregate. These functional consequences are likely to be pleiotropic, heterogeneous, and wide-ranging. Indeed, numerous mechanisms have been proposed by which protein aggregation can influence cellular physiology (Satyal *et al.*, 2000; Trojanowski and Lee, 2000; Bence *et al.*, 2001; Willingham *et al.*, 2003; Balch *et al.*, 2008; Duennwald and Lindquist, 2008). Understanding both substrate-specific and more general downstream consequences (both positive and negative) of protein aggregates is likely to be of importance for fully understanding the pathogenesis of at least some protein-folding disorders.

This article was published online ahead of print in MBoC in Press (http://www.molbiolcell.org/cgi/doi/10.1091/mbc.E10-07-0638) on March 16, 2011.

*Present address: Saha Institute of Nuclear Physics, Sector-1, Block-AF, Room 4622, Bidhannagar, Kolkata 700 064, India.

Address correspondence to: Oishee Chakrabarti (oishee.chakrabarti@saha.ac.in) or Ramanujan S. Hegde (hegder@mail.nih.gov).

Abbreviations used: CFP, cyan fluorescent protein; CRFR1, corticotropin-releasing factor receptor type 1; cyPrP, cytosolic PrP; ER, endoplasmic reticulum; FBS, fetal bovine serum; FRAP, fluorescence recovery after photobleaching; GFP, green fluorescent protein; GPI, glycosylphosphatidylinisotol; Htt, Huntingtin; mFP, monomeric fluorescent protein; Opn, osteopontin; PBS, phosphate-buffered saline; Prl, preprolactin; PrP, prion protein; Ub, ubiquitin.

A common model of aggregate-mediated cellular dysfunction involves sequestration of key cellular factors (Olzscha *et al.*, 2011). For example, aggregates of polyglutamine-expanded mutant proteins in Huntington's disease may sequester essential proteins possessing normal polyQ repeats, including the transcription factors TATA-box binding protein (TBP) and CREB (cAMP response element-binding)-binding protein (CBP) (Nucifora *et al.*, 2001; Schaffar *et al.*, 2004). Studies with cell lines and human disease tissues have elucidated the presence of ubiquitin (Ub) and various components of the 20S proteasome in different misfolded protein aggregates (Lowe *et al.*, 1988; DiFiglia *et al.*, 1997; Alves-Rodrigues *et al.*, 1998; Cummings *et al.*, 1998; Ross and Pickart, 2004). Specific proteins may be depleted in a substrate-selective manner. One recent example is the depletion of a cytosolic Ub ligase, Mahogunin, by cytotoxic forms of the prion protein (PrP) (Chakrabarti and Hegde, 2009). Inclusion bodies are also enriched in proteins involved in diverse cellular processes, suggesting that coaggregation of misfolded, damaged, or mutant proteins with normal cellular proteins could explain both the presence of multiple proteins in inclusion bodies and the toxicity associated with protein aggregation in many neurodegenerative diseases (Satyal *et al.*, 2000; Nucifora *et al.*, 2001; Ravikumar *et al.*, 2004; Zhang *et al.*, 2007). Thus, in these models, aggregates have a toxic "gain of function" by effecting a "loss of function" on another cellular protein or pathway.

More recently, considerable attention has been paid to aggregates influencing general protein homeostasis pathways (Balch *et al.*, 2008). These include the biosynthetic, maturation, quality control, and degradation pathways that together determine the overall protein composition (and hence cellular physiology) at any given moment. It is hypothesized that a subtle shift in any of these pathways (e.g., by slightly reducing the efficacy of quality control) would perturb homeostasis and cause a range of cellular dysfunction (Gidalevitz *et al.*, 2006; Balch *et al.*, 2008; Olzscha *et al.*, 2011). For example, aggregates were shown to perturb the Ub-proteasome system, perhaps by direct inhibition of the proteasome (Bence *et al.*, 2001; Bennett *et al.*, 2005, 2007). More dramatically, aggregates were able to reveal previously masked temperature-sensitive phenotypes (even at the permissive temperature) of various otherwise unrelated mutant proteins (Gidalevitz *et al.*, 2006). The explanation offered for this striking observation was that modestly perturbed maturation and quality control pathways were being revealed by their preferential importance to especially metastable proteins (Olzscha *et al.*, 2011). A similar slight but progressive and physiologically relevant perturbation to the protein homeostasis pathways was also proposed to accompany aging (Cohen *et al.*, 2006; Ben-Zvi *et al.*, 2009). These studies illustrate that even minor perturbations to basic cellular processes can be detected if sufficiently sensitive assays are employed.

Here we describe the serendipitous discovery of a previously unappreciated pathway influenced by cytosolic protein aggregates: the normally rapid degradation of nontranslocated secretory and membrane proteins. These are polypeptides that, despite containing hydrophobic signals for translocation into the endoplasmic reticulum (ER), fail to be properly imported. This failure is typically due to intrinsic inefficiencies in the targeting or translocation reactions (Kim *et al.*, 2002; Levine *et al.*, 2005) but may also be a consequence of regulated translocation (Kang *et al.*, 2006). This nontranslocated population is typically rapidly degraded by a proteasome-dependent pathway (Rane *et al.*, 2004; Besemer *et al.*, 2005; Garrison *et al.*, 2005; Kang *et al.*, 2006). We now find, however, that their degradation can be directly influenced by the presence of cytosolic aggregates without detectable loss of general proteasomal activity. Conversely, in certain specialized circumstances, nontranslocated proteins may actually contribute substantially to aggregate dynamics, facilitating their persistence and growth.

RESULTS AND DISCUSSION

Definitions and nomenclature

This study deals with aggregates, accumulations, nondegraded, and mislocalized proteins. These terms, particularly "aggregate," are variably defined in the literature. It is therefore worth clarifying our usage. In what follows, aggregate indicates an altered state of a protein in which more than the normal number of copies of that protein are coassociated in a manner that changes its biochemical properties. The altered biochemical properties that typify aggregates include reduced solubility, altered (typically increased) protease resistance, higher density (i.e., increased protein per unit volume, as might be visualized by fluorescence), reduced diffusional mobility, and altered (typically decreased) antibody accessibility. Not all of these parameters can be assayed in each circumstance, but one or more of these are used in this study to provide evidence for an aggregated state. Importantly, no additional properties should be inferred by the reader; for example, amyloid or prion states are highly specific types of aggregate.

In cases where we cannot know the aggregated status of a protein, we use other descriptors. "Accumulation" refers to an increased population of a protein than would be observed under normal conditions. "Nondegraded" means a protein or population that under other circumstances would have been degraded (and hence results in accumulation over time). "Mislocalized" indicates a population of a protein that is in a different cellular compartment than the major, normal functional form of that protein. With each of these terms, the protein is not necessarily aggregated, although it certainly could be. Hence in this study the aggregation status should not be inferred in instances where we use these other terms.

Finally, a wide range of PrP variants and other constructs are used in this study. These variants differ in their localization and biochemical properties and, in most cases, have been characterized extensively in earlier studies. To assist the reader, Supplemental Table S1 has been provided. It lists the constructs, their main features, and appropriate references.

A mechanism for "self-perpetuation" of cytosolic PrP aggregates

We began our study by investigating a previous observation of apparent "self-perpetuation" of PrP aggregates in the cytosol (Ma and Lindquist, 2002). In that study, transient proteasome inhibition (for 2 h) led to the generation of a small population of unglycosylated PrP that was relatively insoluble and partially protease resistant, consistent with a cytosolic aggregated species. More surprisingly, removal of the inhibitor not only failed to clear the aggregate, but led to its selective growth and accumulation over time to very high levels. This accumulation was interpreted to mean that the initial seed of the aggregate was in a conformation that led to conversion of newly synthesized PrP into that same conformation, thereby mirroring the prion conversion process that generates infectious prions.

Subsequent studies showed that this cytosolic PrP (cyPrP) is not transmissible, arguing that it had not acquired a conformation that leads to templated conversion (Norstrom *et al.*, 2007). Furthermore, the source of cyPrP was traced primarily to PrP molecules that had failed to enter the ER, and not molecules originating inside the ER (Drisaldi *et al.*, 2003; Rane *et al.*, 2004). In fact, cyPrP generation, even with prolonged proteasome inhibition, could be prevented simply by increasing the efficiency of PrP translocation with another signal sequence (Rane *et al.*, 2004, Kang *et al.*, 2006). Although

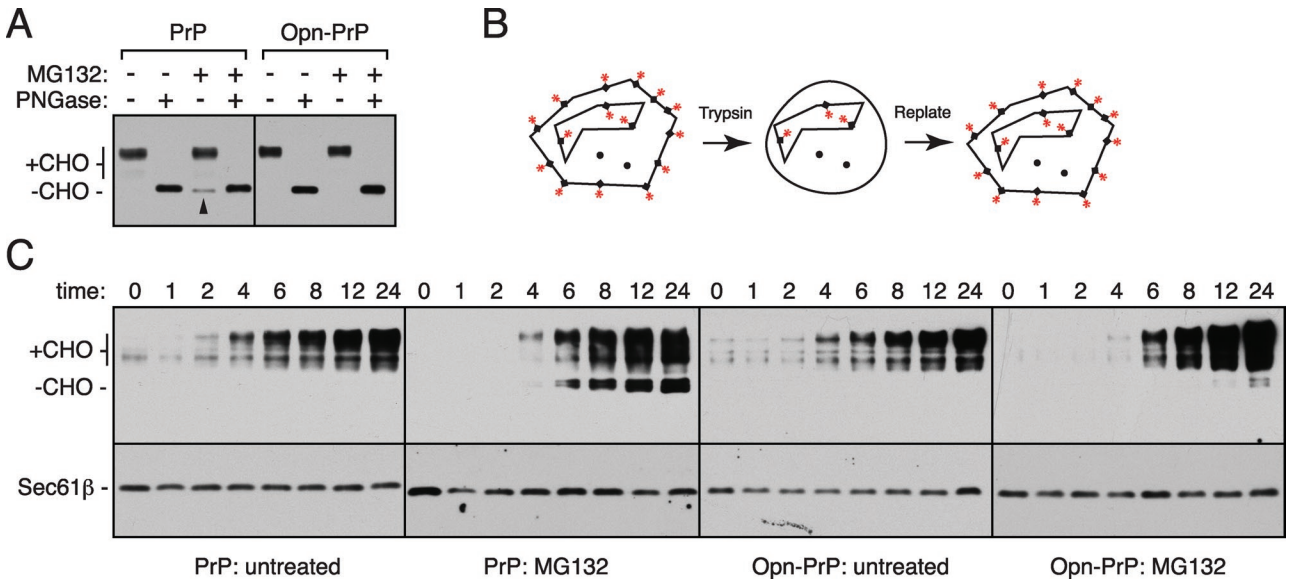

FIGURE 1: Transient proteasome inhibition amplifies nontranslocated PrP aggregates. (A) N2a cells stably expressing either wild-type PrP or Opn-PrP were treated with proteasome inhibitor (5 μM MG132) for 4 h and analyzed by immunoblotting before or after deglycosylation with peptide N-glycosidase F (PNGase F). The arrowhead indicates a nonglycosylated species seen upon proteasome inhibition. (B) Design of experiment shown in panel C. Glycosylated PrP (with red asterisks) on the surface is removed by trypsin, after which only intracellular species are spared. Repopulation of PrP occurs after replating and recovery. (C) PrP or Opn-PrP cells were left untreated or treated with 5 μM MG132 for 4 h, after which they were washed, trypsinized, and replated as eight replicates in inhibitor-free medium. The eight wells were harvested at the indicated times (in hours) after replating and were analyzed by immunoblotting for either PrP (top panels) or Sec61β (bottom panels).

these observations shed light on some aspects of cyPrP biosynthesis and degradation, they didn't explain the apparent "propagation." To investigate this issue, we revisited the proteasome inhibition experiments using stable cell lines expressing either wild-type PrP or osteopontin (Opn)-PrP at levels comparable to endogenous PrP in brain (Kang *et al.*, 2006). The latter is a version of PrP containing the highly efficient signal sequence from Opn (Kim *et al.*, 2002), and therefore generates little nontranslocated cyPrP (Rane *et al.*, 2004, 2010).

We confirmed that, as with transient transfection, stable PrP-expressing cells generate an unglycosylated form upon short term (4 h) proteasome inhibition with MG132 (Figure 1A). This unglycosylated species was due to stabilization of nontranslocated PrP because it was not seen with Opn-PrP–expressing cells (Figure 1A) and because it was shown in earlier studies to contain an uncleaved signal sequence (Drisaldi *et al.*, 2003; Rane *et al.*, 2004; Orsi *et al.*, 2006). We further verified that this species was intracellular (as judged by inaccessibility to extracellular trypsin) and detergent insoluble (unpublished data), again consistent with earlier observations of transiently transfected cells (Ma and Lindquist, 2002; Drisaldi *et al.*, 2003; Rane *et al.*, 2004; Orsi *et al.*, 2006). Thus, in stable cells expressing PrP at moderate levels, a small population of nontranslocated species is constantly being generated in the cytosol and degraded by the proteasome. Inhibition of the proteasome stabilizes this species, and generates a "seed" of cyPrP that appears to be aggregated.

We next performed transient proteasome inhibition and recovery experiments to investigate the consequences of this seed of nontranslocated PrP aggregates. Between the initial treatment and recovery, the cells were trypsinized and replated (Figure 1B). This experimental procedure removed mature PrP from the cell surface, ensured complete removal of the proteasome inhibitor, allowed the visualization of intracellular PrP, and permitted us to assay the subsequent rate of repopulation of PrP by new synthesis. In untreated cells, essentially all PrP at steady state was surface exposed, and hence not seen after trypsin treatment. The small amount that is observed was likely in intracellular compartments of the secretory pathway, because its glycans are not fully mature. A major mature glycosylated species was repopulated over the course of 24 h (Figure 1C). Identical results were obtained for Opn-PrP (Figure 1C), and, in both cases, a long-lived intracellular membrane protein (Sec61β) was unaffected by trypsin treatment or recovery. On treatment of PrP-expressing cells with MG132 (for 4 h) and extracellular trypsin digestion, very small amounts of intracellular pools were observed. Only on long exposures was an unglycosylated species seen (unpublished data). During recovery, however, unglycosylated species accumulated over time along with the glycosylated mature species (Figure 1C). These unglycosylated species were almost exclusively from nontranslocated PrP as they were barely observed with Opn-PrP cells treated under identical conditions (Figure 1C). Similar results were obtained in cells transiently transfected with PrP or Opn-PrP (unpublished data; see also Rane *et al.*, 2004). Furthermore, a different efficient signal sequence (from preprolactin [Prl]) fused to PrP (Prl-PrP) also abolished the generation of unglycosylated species of PrP in similar proteasome inhibition/recovery experiments (unpublished data). These observations suggested that nontranslocated PrP failed to be effectively degraded in proteasome-pretreated cells, despite removal of the proteasome inhibitor.

To verify this conclusion, we performed pulse-chase studies of PrP to directly examine the fate of the nontranslocated population. Unlike at steady state, when nontranslocated PrP is usually undetectable (e.g., Figure 1), pulse labeling (for 30 min) showed that ~5–10% of newly synthesized PrP fails translocation and contains an unprocessed signal sequence (Figure 2A, lane 1; quantified in

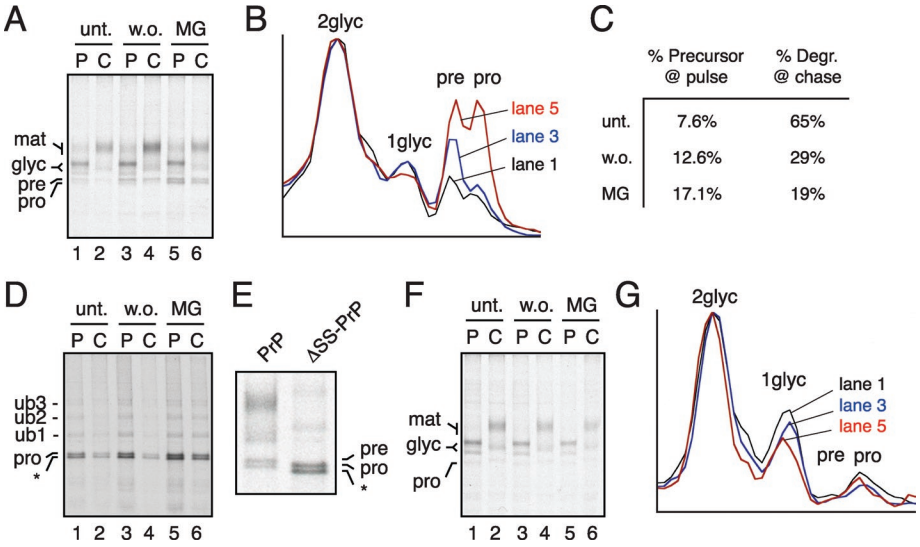

FIGURE 2: PrP precursor is selectively stabilized in proteasome inhibitor–pretreated cells. (A, D, and F) Pulse-chase analyses of PrP (A), ΔSS-PrP (D), and Opn-PrP (F). Pulse-labeling with ^{35}S-Met was for 30 min (lanes 1, 3, and 5), followed by chase for 1 h (lanes 2, 4, and 6). The pulse-chase was performed on either untreated cells (unt; lanes 1 and 2), in the continuous presence of 5 μM MG132 (MG; lanes 5 and 6), or on cells 4 h after a 4-h MG132 treatment was washed out (w.o.; lanes 3 and 4). Mature (mat), core-glycosylated species (glyc), precursor (pre), and processed (pro) species of PrP are indicated. For ΔSS-PrP, ubiquitinated species can also be observed (ub1, ub2, etc.). A partially digested species is also indicated with an asterisk. Panels B and G show densitometric traces of the pulse lanes for untreated (black), MG132 (red), and washout (blue) samples for the experiments in panels A and F, respectively. (C) Quantitation of the experiment in panel A. The percentage of total PrP generated in the precursor form during pulse-labeling, and the amount of its degradation during the chase, are shown. (E) Comparison of migration on SDS–PAGE of pulse-labeled PrP vs. ΔSS-PrP. Note that the top band of ΔSS-PrP comigrates with the processed species observed for PrP, whereas the precursor form of PrP migrates slightly slower. The asterisk indicates a partially digested form of cyPrP that is generated by yet unknown cytosolic proteases (see also Figure 3A).

Figure 2, B and C; see also Rane *et al.*, 2004; Kang *et al.*, 2006; Orsi *et al.*, 2006). The remainder of pulse-labeled PrP is core-glycosylated upon its initial synthesis. During a 1-h chase (Figure 2A, lane 2), core-glycosylated PrP matures to higher molecular weight forms due to glycan modifications in the Golgi. By contrast, most (~65%) of the nontranslocated precursor PrP is degraded during the chase (Figure 2C). In the continuous presence of proteasome inhibitor, core glycosylation and maturation remained normal (Figure 2A, lanes 5 and 6; Figure 2B). The nontranslocated precursor species of PrP, however, was now stabilized: Not only was it more readily visible during the pulse-labeling (Figure 2, A–C), only ~19% was degraded during the chase (Figure 2C). Note that two forms of unglycosylated PrP are observed: These two forms appear to correspond to signal-uncleaved and -cleaved forms (Orsi *et al.*, 2006). The latter may arise due to either dislocation of misfolded PrP from the ER lumen, cotranslational slippage of nascent PrP into the cytosol after its signal has been processed in the ER, or some unidentified cytosolic processing of nontranslocated PrP. In any case, this form is also stabilized in the presence of proteasome inhibitor.

In cells that had been treated with proteasome inhibitor but subsequently returned to normal conditions, the signal-uncleaved form of nontranslocated PrP (i.e., precursor) was preferentially stabilized (Figure 2A, lanes 3 and 4; see densitometry trace in Figure 2B), with only ~29% degraded during the chase (Figure 2C). This finding suggests that, in transiently inhibited cells, the fate of the nontranslocated population of PrP containing an unprocessed signal sequence is selectively altered: Rather than being degraded by the proteasome, it is now stabilized. This stabilization was not due to a lack of reversal of proteasome inhibition because a PrP construct lacking a signal sequence (ΔSS-PrP; Ashok and Hegde, 2008; Rane *et al.*, 2008) was degraded normally in comparably treated cells (Figure 2D, lanes 3 and 4), and stabilized only when proteasome inhibitor was continuously present throughout the pulse-chase (Figure 2D, lanes 5 and 6). Thus only the species of PrP containing an unprocessed signal sequence is stabilized in transiently inhibited cells, despite return of proteasome activity. As expected, Opn-PrP did not generate easily detectable nontranslocated PrP (Figure 2, F and G), consistent with its highly efficient translocation into the ER (Rane *et al.*, 2004; Levine *et al.*, 2005; Kang *et al.*, 2006). It is worth noting that MG132 could, either directly or indirectly (e.g., by inducing acute ER stress; Kang *et al.*, 2006), influence translocation into the ER of proteins with certain signal sequences. This seems unlikely, however, because in the time frames and experimental conditions analyzed here, we have not detected evidence of acute ER stress (unpublished data). For example, translation was not notably attenuated in the presence or absence of MG132 treatment (Figure 2, A, D, and F). Furthermore, quantitation of the pulse-chase experiment (Figure 2C) suggests that the increase in precursor PrP can be explained largely by its decreased degradation during the 30-min labeling period. Hence, although translocational inhibition could contribute partially to cyPrP aggregate growth, the primary mechanism seems to involve stabilization of the basally generated nontranslocated PrP precursor.

Curiously, cyPrP lacking the signal sequence (ΔSS-PrP) and/or the glycosylphosphatidylinisotol (GPI)-anchoring sequence (ΔSSΔGPI-PrP), while accumulating upon proteasome inhibition (Figure 3A, lanes 5 and 6) and apparently aggregated as judged by detergent solubility (Figure 3B, lanes 5 and 6), does not continue to grow and accumulate upon removal of the inhibitor (Figure 3C). This result could be explained if aggregates of ΔSS-PrP and ΔSSΔGPI-PrP are more rapidly turned over (e.g., by autophagy) than those formed by PrP precursor. Alternatively, the degradation of newly synthesized ΔSS-PrP and ΔSSΔGPI-PrP may be impervious to preexisting aggregates, whereas degradation of precursor PrP is selectively delayed in the presence of preexisting aggregates. Of these possibilities, we favor the latter based on direct analysis of newly synthesized precursor PrP and ΔSS-PrP by pulse-chase analysis (Figure 2, A and D, respectively). Furthermore, the observation that ΔSS-PrP and ΔSSΔGPI-PrP are stabilized to a similar extent as precursor PrP upon proteasome inhibition (Figure 3A) suggests that turnover of these three species by autophagy pathways is probably comparably slow. We therefore conclude that, in the presence of preexisting aggregates, precursor PrP is preferentially delayed in its normally rapid proteasomal degradation. This delay apparently leads to

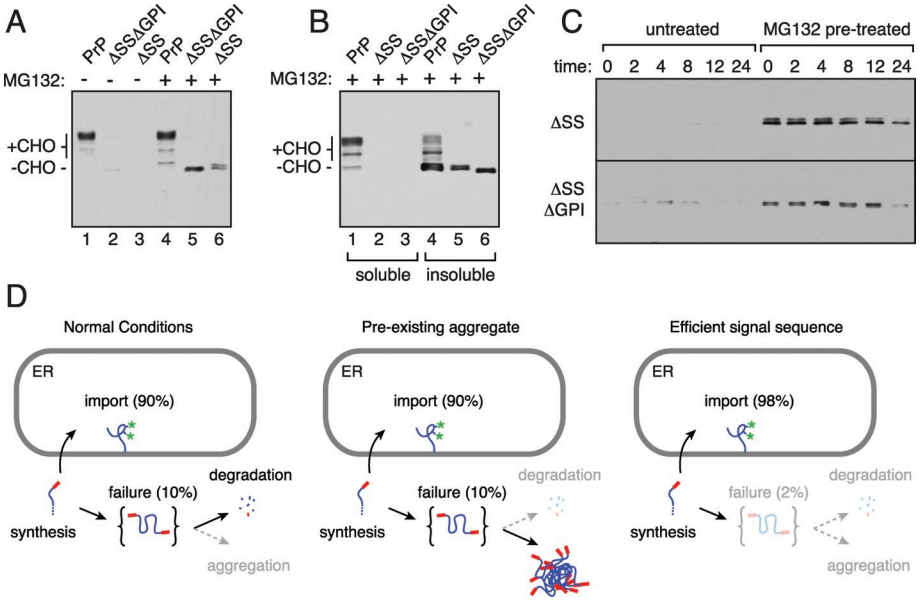

FIGURE 3: cyPrP aggregates lacking a signal sequence do not propagate. (A) Cells transiently transfected with PrP, ΔSS-PrP, or ΔSSΔGPI-PrP were analyzed by immunoblotting before and after treatment with 5 μM MG132 for 4 h. (B) Cells treated for 6 h with 5 μM MG132 were separated into a detergent-soluble and -insoluble fraction before analysis. Twice the relative amount of insoluble fraction was loaded compared with the soluble fraction. (C) ΔSS-PrP and ΔSSΔGPI-PrP were analyzed by the replating assay as in Figure 1C. Note that although unglycosylated species are clearly stabilized by proteasome inhibition, this species does not get amplified upon inhibitor removal and recovery. (D) Model for apparent "propagation" of cyPrP aggregates. The left panel shows PrP biosynthesis under normal conditions, where ~90% of synthesized polypeptides are correctly imported into the ER, whereas ~10% are nontranslocated precursors that are rapidly degraded in the cytosol. In the presence of preexisting aggregates (middle panel), the precursor molecules containing a signal sequence (red) are preferentially recruited into the aggregate instead of degradation. This aggregation can be largely averted by improving translocation into the ER with an efficient signal sequence (right panel).

aggregation as judged by its relative insolubility in detergent solutions. Aggregation would further exacerbate the situation, leading to the apparent "self-conversion" phenomenon (see model in Figure 3D).

It should be noted that, although the signal-containing nontranslocated PrP is clearly the main (or only) species that contributes to aggregate propagation (as evidenced by the pulse-chase), the nonglycosylated bands that accumulate over time are heterogeneous (see, e.g., Figure 1C). This mixed population appears to be the consequence of some proteolytic trimming or processing. Because this consequence was also seen for ΔSS-PrP (e.g., Figure 2, D and E, and Figure 3, A and C), the processing is likely to be occurring in the cytosol, although we cannot rule out processing in another compartment after partial translocation by an unusual mechanism. Regardless of the source of processing, the final processed product migrates closely to ΔSSΔGPI-PrP (Figure 3A). This result explains the previous suggestion (based on migration in SDS–PAGE) that the "self-propagating" species of PrP had the N- and C-terminal signals removed (Ma and Lindquidst, 2002). Although that had been interpreted to indicate transit through the ER lumen, this conclusion may not be correct because there seem to be alternative mechanisms for generating a similarly migrating product. Thus we conclude that "self-propagation" can be explained by selective stabilization of unprocessed nontranslocated PrP in the presence of preexisting cyPrP aggregates generated by transient proteasome inhibition (Figure 3D).

Colocalization of nontranslocated PrP with cyPrP aggregates in live cells

While the "self-propagation" of PrP proved to be unrelated to prion replication, our investigation of this phenomenon revealed an unexpected finding: Nontranslocated PrP is especially prone to stabilization in the presence of preexisting aggregates. To validate and extend this conclusion, we sought to visualize this phenomenon directly in live cells in the absence of proteasome inhibitor treatments. This visualization not only minimized potential confounding effects of proteasome inhibitors (such as changes in PrP mRNA, depletion of cellular Ub pools, induction of ER stress, or translational attenuation), but allowed us to spatially localize the stabilized population of nontranslocated PrP. We therefore expressed monomeric fluorescent protein (mFP)-tagged wild-type PrP (PrP-mFP) in cells containing aggregates of cyPrP tagged with a different colored mFP.

To generate fluorescent cyPrP aggregates, we N-terminally tagged a version of PrP (in particular, PrP residues 40–231) lacking both its N-terminal signal sequence and C-terminal GPI-anchoring signal. Such mFP-$PrP_{40–231}$ constructs efficiently produce readily visible cytosolic and nuclear aggregates in nearly all cells (Chakrabarti and Hegde, 2009). N2a cells expressing PrP-mCFP (cyan fluorescent protein) with or without mRFP-$PrP_{40–231}$ were analyzed by microscopy at various times after transfection. In the absence of cytosolic aggregates, PrP-mCFP localizes to the cell surface and perinuclear structures of the secretory pathway, including Golgi and endosomes, closely mirroring untagged PrP (Rane *et al.*, 2004). In cells containing aggregates of mRFP-$PrP_{40–231}$, PrP-mCFP was typically unaffected in its localization. In ~12.2% of cells, however, a subpopulation of PrP-mCFP clearly colocalized with the mRFP-$PrP_{40–231}$ aggregates to varying extents (Figure 4A). In some cells, PrP-mCFP was largely on the rim of aggregates, whereas in other instances, it was more homogeneously incorporated. Aggregates in the cytoplasm as well as nucleus were able to recruit PrP-mCFP. The latter unambiguously illustrates that the colocalizing population of PrP-mCFP is not in the secretory pathway. Colocalization could be observed beginning as early as 8 h, when PrP-mCFP fluorescence was first clearly visible, and was observed in cells of varying expression levels (unpublished observations). Importantly, the colocalization was not influenced by choice of FPs, as different combinations gave the same results (unpublished data), and an FP expressed in the cytosol did not coaggregate with the cyPrP aggregates (Supplemental Figure S1; see also Chakrabarti and Hegde, 2009).

Colocalization of PrP-mCFP with mRFP-$PrP_{40–231}$ was largely eliminated (to 2.5% of cells) by replacing the PrP signal sequence with the more efficient signal sequence from prolactin (termed Prl-PrP-mCFP) (Figure 4B). Even in the most highly expressing cells, Prl-PrP-mCFP was found only in the secretory pathway, clearly segregated from mRFP-$PrP_{40–231}$ aggregates. Similar results were obtained when the Opn signal sequence was used (unpublished

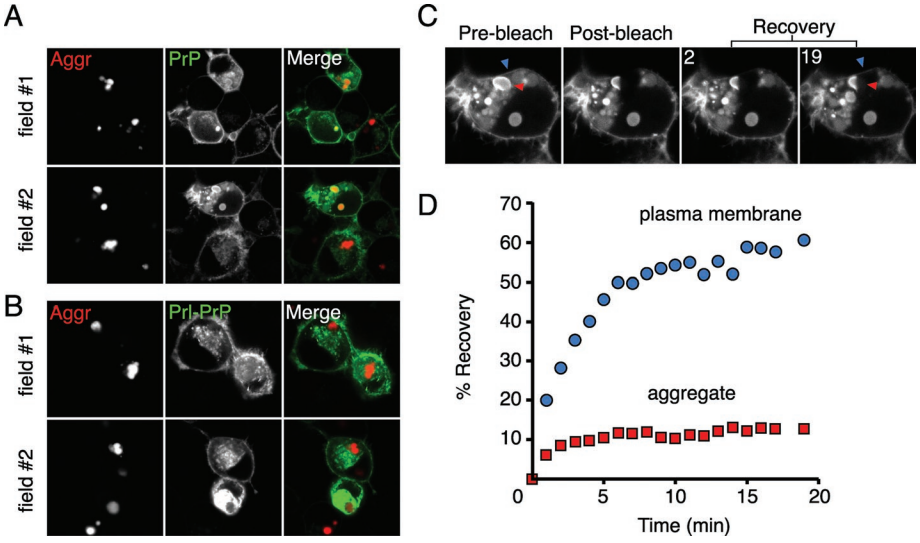

FIGURE 4: Nontranslocated PrP coaggregates with cyPrP aggregates in live cells. (A) Cells cotransfected with mRFP-$PrP_{40–231}$ (the aggregates visualized in the red channel) and PrP-CFP (green channel) were visualized ~24–30 h after transfection. Individual channels and the merged images of two fields are shown. (B) As in panel A, but with Prl-PrP-CFP. Images were collected at the same time as in panel A, and with identical imaging settings. Note that with Prl-PrP, little or no coaggregation was evident, even in the grossly overexpressing cell in field #2. (C) An aggregate-containing cell from panel A (in field #2) was analyzed by FRAP of wild-type PrP-CFP. A region containing approximately half of an apparent aggregate (red arrowhead) as well as a section of the plasma membrane (blue arrowhead) was photobleached, and monitored for 20 min at 1-min intervals. Shown are the images immediately before and after the photobleaching, as well as after 2 and 19 min of recovery. Note that the thin rim of fluorescence at the plasma membrane has recovered in the 19-min image (blue arrowhead), but the aggregate (red arrowhead) remains bleached even at 19 min. Images are shown only in the CFP channel. Similarly bleaching the mRFP-$PrP_{40–231}$ resulted in no recovery (Supplemental Figure S2). (D) Recovery of fluorescence at the plasma membrane (blue circles) and aggregate (red squares) after photobleaching from the experiment in panel C.

data). Previous analyses have shown that the Prl and Opn signal sequences are highly efficient in vivo (Kim *et al.*, 2002; Rane *et al.*, 2004, 2010; Levine *et al.*, 2005), with little nontranslocated PrP (<5%). In contrast, the slightly inefficient signal sequence of PrP leads to ~10–20% nontranslocated species in the cytosol (Kim *et al.*, 2002; Rane *et al.*, 2004, 2010; Levine *et al.*, 2005). That efficient signal sequences markedly reduce the degree of colocalization strongly suggests that the major population of PrP-mCFP that colocalizes with mRFP-$PrP_{40–231}$ arises from nontranslocated polypeptides. Although it is possible that PrP-mCFP dislocated from the ER also contributes to colocalization, it seems unlikely. If this retrotranslocated population were a significant contributor to coaggregation, it would not have been eliminated by increasing signal sequence efficiency because with both signals the vast majority of the PrP is translocated into the ER. It is worth noting that the Prl signal sequence is probably not perfect, because some coaggregation of Prl-PrP-mCFP with mRFP-cyPrP was observed eventually in the highest expressing cells (unpublished data). Thus, consistent with the biochemical experiments using the proteasome inhibitor paradigms, we find that nontranslocated PrP is preferentially stabilized in cells containing cyPrP aggregates, with which it partially colocalizes.

To determine whether the nontranslocated population of PrP-mCFP that colocalizes with aggregates of mRFP-$PrP_{40–231}$ is itself aggregated, we analyzed its diffusional mobility using fluorescence recovery after photobleaching (FRAP; Snapp *et al.*, 2003). As a control for an immobile protein, we also performed FRAP on the mRFP-$PrP_{40–231}$ aggregate, while the plasma membrane population of PrP-mCFP served as a control for nonaggregated diffusionally mobile protein. After photobleaching, PrP-mCFP on the plasma membrane (blue arrowhead, Figure 4C) recovered with a $t_{1/2}$ of ~2–3 min, as expected for a GPI-anchored membrane protein (Figure 4, C and D; Supplemental Figure S2). In contrast, little or no recovery was observed over a 19-min period for the PrP-mCFP population on the surface of the intracellular aggregates (red arrowhead, Figure 4, C and D; Supplemental Figure S2). This was the case whether one section of an aggregate or an entire aggregate was photobleached, indicating minimal exchange of PrP-mCFP within the aggregate or between the aggregate and other cellular pools (unpublished data). As expected, photobleached mRFP-$PrP_{40–231}$ did not recover within the 19-min experiment (Supplemental Figure S2). We therefore conclude that the PrP-mCFP that colocalizes with the mRFP-$PrP_{40–231}$ aggregate is diffusionally restricted, suggesting that it is aggregated there. Thus preexisting mRFP-$PrP_{40–231}$ aggregates substantially influence the fate of nontranslocated PrP-mCFP without noticeably altering the population that transits through the secretory pathway.

Accumulation of nontranslocated PrP in aggregate-containing cells

We also attempted to visualize untagged wild-type PrP coaggregating with mCFP-$PrP_{40–231}$ by indirect immunofluorescence at various times after transfection. Consistent coaggregation could not be detected reliably, apparently due to poor antibody access (as even FP-tagged PrP in the aggregate was not decorated effectively by anti-PrP antibodies; see Supplemental Figure S3). Nonetheless, varying amounts of increased intracellular accumulation of PrP was observed in ~20% of cells containing cytosolic mCFP-$PrP_{40–231}$ aggregates (Table 1; see Figure 5 for examples). Experiments expressing wild-type PrP without mCFP-$PrP_{40–231}$ showed aberrant increased intracellular accumulations in fewer than 5% of cells (Table 1). At later times (3 d), gross alteration of cell morphology was observed in some of the aggregate-containing cells. Remarkably, the increased accumulation and altered cellular morphology were seen far less frequently in Prl-PrP–expressing cells, suggesting that these effects can be ascribed to nontranslocated PrP (Figure 5 and Table 1).

These results suggest that the nontranslocated populations of both FP-tagged and -untagged PrP are altered in their degradation in cells containing cyPrP aggregates. Although coaggregation could not be directly visualized with untagged PrP, its accumulation was nonetheless readily apparent and could be traced to the slight inefficiency of the native PrP signal sequence. At present, the precise aggregation state and localization of the accumulated nontranslocated PrP has not been fully characterized. The fact that it occurs in only a subset of cells complicates biochemical analyses, and the absence of an FP tag prevents the use of live cell diffusion analysis. These limitations notwithstanding, we can still conclude that the normally minor and transient

	PrP			Prl-PrP	CRFR1			Prl-CRFR1
	24 h	48 h	96 h	96 h	24 h	48 h	96 h	96 h
$PrP_{40–231}$	21% (32/151)	22% (48/216)	30% (39/130)	3.9% (9/232)	19% (44/235)	22% (22/98)	19% (25/133)	6.4% (11/172)
Htt_{Q103}	n.d.	n.d.	25% (29/115)	6.0% (8/133)	n.d.	n.d.	20% (25/128)	6.5% (10/155)
None	n.d.	3.8% (5/129)	n.d.	n.d.	n.d.	5.5% (7/126)	n.d.	n.d.

TABLE 1: Quantification of aggregate-induced intracellular accumulation. The aggregated protein indicated at left was coexpressed with the test protein indicated along the top. At each time point, the % of aggregate-containing cells that showed excess intracellular accumulation of the test protein is indicated. The raw values are shown in parentheses. n.d., not determined.

population of nontranslocated PrP can be "amplified" to high levels by preexisting aggregates of cyPrP that apparently preclude its efficient degradation.

Nontranslocated membrane proteins accumulate in aggregate-containing cells

Earlier studies of both isolated signal sequences and native proteins suggested that PrP is not unusual in displaying slightly inefficient translocation and raised the possibility that the observations mentioned earlier in the text regarding nontranslocated PrP might also apply to other proteins. One native protein with a slightly inefficient signal sequence is corticotropin-releasing factor receptor type 1 (CRFR1), a G protein–coupled receptor (Kang *et al.*, 2006). Indeed, a nonglycosylated form of CRFR1 accumulated upon proteasome inhibition, and this accumulation was substantially reduced upon replacement of the native signal sequence with that from Prl (Figure 6). Normally, CRFR1 localizes to the cell surface and various intracellular membranous structures, consistent with its trafficking through the secretory pathway (e.g., Figures 7 and 8B). In cells containing mCFP-$PrP_{40–231}$ aggregates, we observed increased intracellular accumulation of CRFR1 in ~20% of cells (Table 1; examples in Figure 7). This intracellular accumulation was observed in fewer than 6% of cells lacking mCFP-$PrP_{40–231}$ aggregates (Table 1). Importantly, replacing the signal sequence of CRFR1 with that from Prl (Prl-CRFR1) reduced the fraction of cells containing intracellular accumulations approximately threefold (Table 1). These findings suggest that preexisting aggregates of one protein (mCFP-$PrP_{40–231}$) can influence the fate of the nontranslocated population of an unrelated protein in the cytosol to cause its accumulation over time.

To generalize this conclusion, we examined the fate of both PrP and CRFR1 in cells expressing a qualitatively different type of aggregate generated by the polyglutamine-expanded exon 1 of Huntingtin (Htt). Green fluorescent protein (GFP)-Htt_{Q103} with a poly-Q repeat of 103 residues forms aggregates in the cytoplasm and nuclei of ~12–15% of cells (Robinson *et al.*, 2008). When coexpressed with these Htt aggregates, PrP and CRFR1 were observed by immunofluorescence to accumulate as amorphous structures in the cytoplasm of ~20% of cells containing Htt_{Q103} aggregates (Table 1; Figure 8, A and B). This accumulation was observed approximately threefold less frequently for Prl-PrP or Prl-CRFR1 analyzed in parallel (Table 1). Thus, for two unrelated signal-containing proteins, we find that the nontranslocated polypeptides are altered in their degradation in cells containing either of two unrelated cytosolic aggregates.

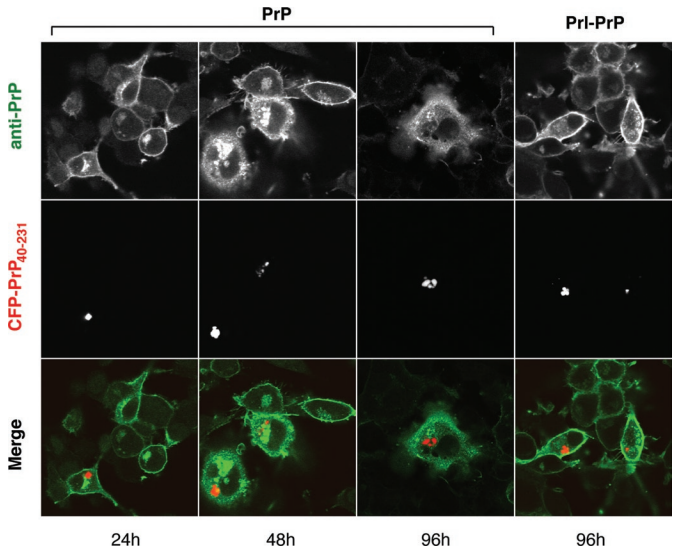

FIGURE 5: Nontranslocated PrP stabilization by cyPrP aggregates. Cells cotransfected with mCFP-$PrP_{40–231}$ and either PrP or Prl-PrP were cultured for between 24 and 96 h before analysis by indirect immunofluorescence with 3F4 antibody against PrP. Prl-PrP remains mostly surface localized in most (>90%) cells (see Table 1); a representative example is shown. By contrast, PrP shows a more heterogeneous distribution of staining patterns with varying amounts of intracellular accumulations. A gallery of three images illustrating this heterogeneity is shown, with quantitation of cells with altered localization presented in Table 1. Note that various cells lacking visible aggregates are seen in the images to show the normal, primarily cell-surface localization typical for PrP.

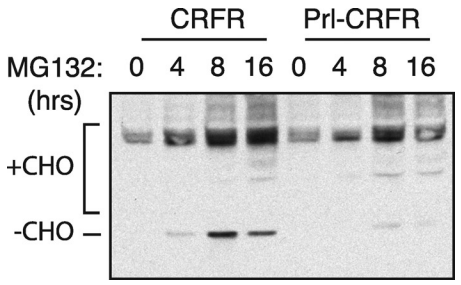

FIGURE 6: Nontranslocated CRFR accumulates upon proteasome inhibition. Cells transiently transfected with CRFR or Prl-CRFR (each tagged with a 12-residue epitope recognized by the 3F4 monoclonal antibody) were treated with 10 μM MG132 for the indicated time periods and analyzed by immunoblotting. Unglycosylated CRFR upon proteasome inhibition is observed to a lesser extent with the Prl signal sequence.

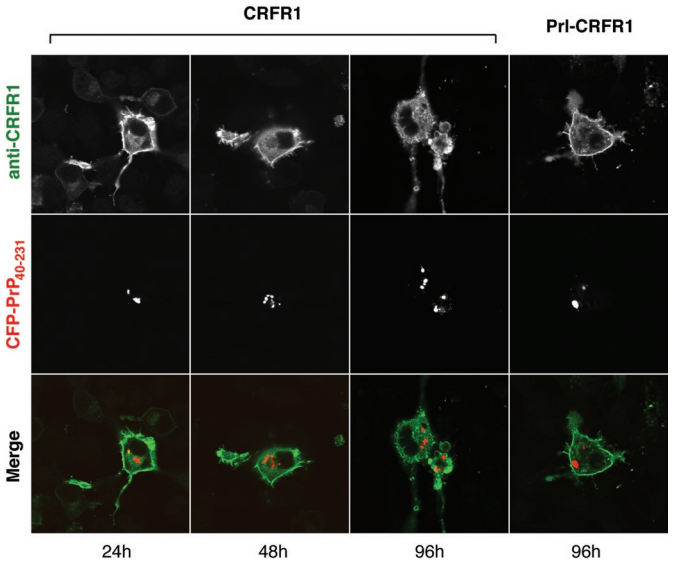

FIGURE 7: cyPrP aggregates stabilize nontranslocated CRFR1. Cells cotransfected with mCFP-$PrP_{40–231}$ and either CRFR1 or Prl-CRFR1 were cultured for 24–96 h before analysis by indirect immunofluorescence with 3F4 antibody. Representative examples of staining patterns for CRFR1 and Prl-CRFR1 are shown, with quantification in Table 1. The left and right images show essentially normal (primarily surface) localization, and the two middle images show either a mixed surface/intracellular or completely intracellular localization pattern.

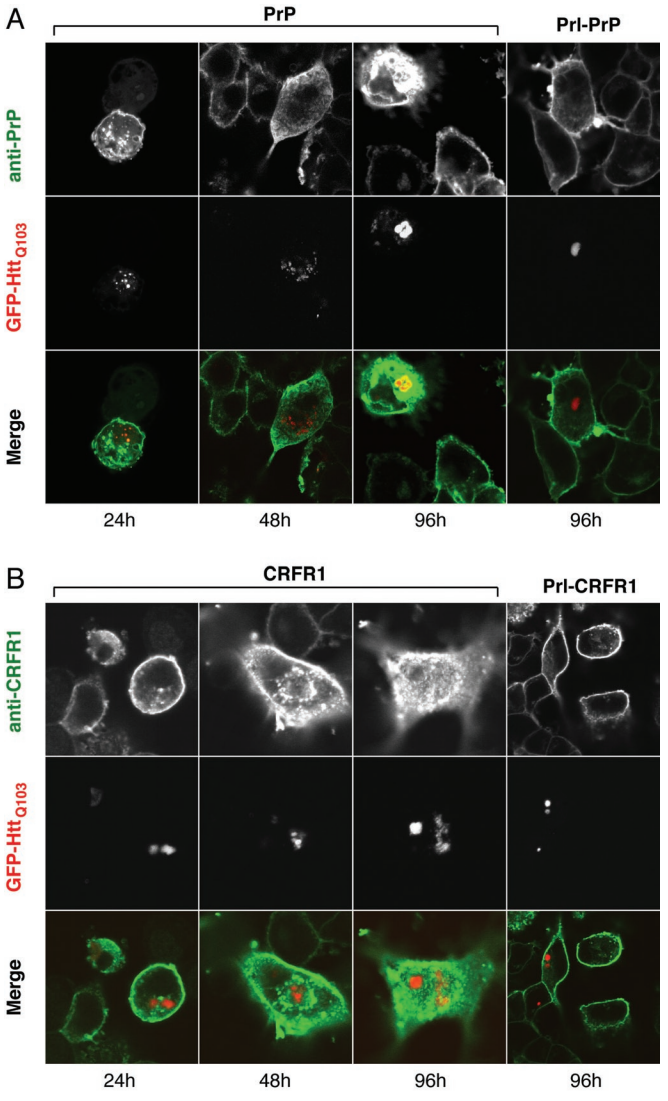

FIGURE 8: Cytosolic Htt_{Q103} aggregates stabilize nontranslocated proteins. (A) An experiment as in Figure 7 was performed, but using GFP-Htt_{Q103} as the cytosolic aggregate and PrP or Prl-PrP as the test proteins. (B) As in panel A, using GFP-Htt_{Q103} as the cytosolic aggregate and CRFR1 or Prl-CRFR1 as the test proteins. Quantitation of the results is shown in Table 1.

Delayed degradation does not require coaggregation

What is the basis of selective stabilization and accumulation of nontranslocated PrP and CRFR1 by cytosolic aggregates? Based on the data presented earlier in the text, it is difficult to distinguish the order of events between two possibilities. In one model, preexisting aggregates might *directly* stabilize newly synthesized nontranslocated precursors by coaggregation, thereby sequestering them away from the degradation machinery. Alternatively, preexisting aggregates could inhibit the degradation machinery, thereby *indirectly* stabilizing nontranslocated precursors that might subsequently aggregate. The hydrophobic and aggregation-prone nature of both PrP and CRFR1 made distinguishing among between possibilities difficult because stabilization and coaggregation seem to occur almost simultaneously. We therefore turned to a simplified substrate in which the highly soluble and autonomously folding GFP was targeted to the ER by an N-terminal signal sequence and C-terminal KDEL signal. Because of its solubility, we reasoned that it may not necessarily be recruited into aggregates. Our goal was to ask whether the fate of the nontranslocated population of this artificial protein was influenced by the presence or absence of cytosolic aggregates and, if so, whether this depends on coaggregation.

The signal sequences plus the first ten mature residues (indicated by "SS+10") of PrP or Prl were appended to the N terminus of mGFP containing a C-terminal KDEL sequence. In preliminary experiments, we confirmed that these signal-containing constructs are normally localized to the ER (unpublished data). These constructs were then coexpressed with cytosolic mRFP-$PrP_{40–231}$ aggregates and observed at 24 and 48 h after transfection (Figure 9). At 24 h posttransfection, most cells (>90%) expressing each of the constructs localized as expected in a nonnuclear reticular pattern consistent with the ER. Evidence of coaggregation with mRFP-$PrP_{40–231}$ was not observed. At 48 h posttransfection, the construct containing the PrP signal sequence (PrP(SS+10)-GFP_{KDEL}) now behaved aberrantly, with a substantial proportion of the expressed protein being distributed diffusely in the nucleocytoplasmic compartment in addition to its expected ER localization. This phenomenon was observed in ~65% of cells containing mRFP-$PrP_{40–231}$ aggregates (n = 54), and was especially prominent in more highly expressing cells. The phenomenon was seen far less frequently for Prl(SS+10)-GFP_{KDEL} (in ~12.5% of aggregate-containing cells; n = 40) and was limited to high expressing cells. As controls, matched constructs lacking the signal sequences were localized diffusely in the nucleocytoplasmic compartment and seemed unaffected by the mRFP-$PrP_{40–231}$ aggregates (Supplemental Figure S4). Little or no evidence of coaggregation was detected for any of the constructs but was most readily observed in the split images, where GFP fluorescence was not enriched (and was often excluded from) the cytosolic region containing the aggregate (Figure 9; Supplemental Figure S4).

These observations lead to three important conclusions. First, the fate of a totally artificial signal-containing protein

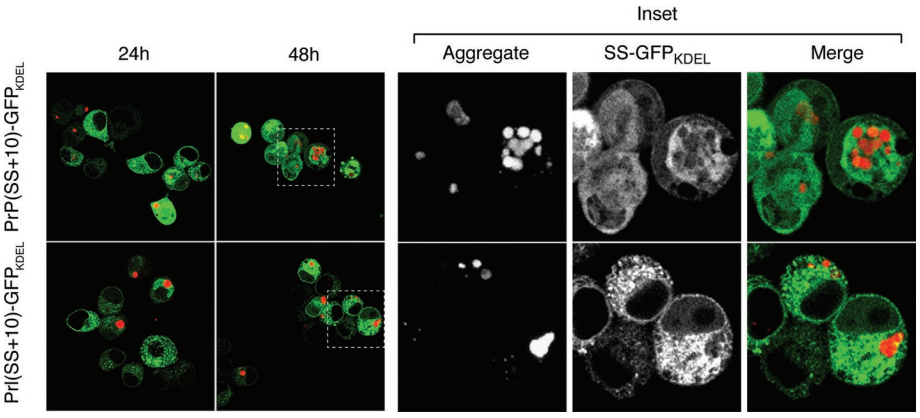

FIGURE 9: Nontranslocated soluble proteins are stabilized in aggregate-containing cells. Cells cotransfected with mRFP-PrP$_{40–231}$ (red) and the indicated signal sequence-GFP-KDEL fusion constructs (green) were imaged after 24 and 48 h. Wide-field images of cells show that at 24 h, the GFP fluorescence is essentially all ER-localized, with clear exclusion from the nucleus. At 48 h, PrP(SS+10)-GFP$_{KDEL}$ now displays substantial nucleocytoplasmic localization. Localization is considerably lower for Prl(SS+10)-GFP$_{KDEL}$, where only the highest expressing cells show some nuclear localization. Inset reveals the localization pattern and illustrates lack of obvious coaggregation of GFP with mRFP-PrP$_{40–231}$.

[PrP(SS+10)-GFP$_{KDEL}$] is influenced by an unrelated cytosolic aggregate. Second, this effect can be largely averted by a matched construct containing a highly efficient signal sequence [Prl(SS+10)-GFP$_{KDEL}$]. This result suggests that the nontranslocated population of PrP(SS+10)-GFP$_{KDEL}$ is being stabilized in the presence of the aggregate. Third, this stabilization of nontranslocated protein is not dependent on its cosequestration with the aggregate, suggesting that stabilization occurs by an indirect mechanism. We cannot exclude the possibility that a subpopulation of nontranslocated GFP is coaggregated but is not visualized because the GFP is misfolded. Even in this scenario, however, it is clear that coaggregation is not an absolute prerequisite for stabilization as a nonaggregated population was readily visualized.

Absence of proteasome inhibition in aggregate containing cells

The observation that stabilization of nontranslocated PrP(SS+10)-GFP$_{KDEL}$ does not require its coaggregation suggests that its degradation pathway is not functioning normally. The simplest explanation would be if the proteasome were being inhibited by the aggregates, as has been suggested in earlier studies (Bence *et al.*, 2001; Bennett *et al.*, 2005). An alternative (but not mutually exclusive) possibility is that other aspects of cytosolic quality control, which still remains poorly understood, might be perturbed. This possibility is also consistent with recent studies suggesting that aggregates can generally influence protein homeostasis pathways (Huang *et al.*, 1998; Schaffar *et al.*, 2004; Gidalevitz *et al.*, 2006).

To investigate this issue, we used a Ub-GFP fusion protein to monitor proteasome activity in cells containing or lacking aggregates (Dantuma *et al.*, 2000). Characterization of this reporter in our cell culture conditions showed that, by immunoblotting, even low-level proteasome inhibition for short periods of time led to detectable increases in reporter stabilization (Figure 10, A and B). The stabilized protein is not seen as a Ub ladder for reasons that are not entirely clear but may involve highly active deubiquitination enzymes or possibly Ub chain addition en bloc instead of sequentially (Li *et al.*, 2007). A wide range of an at least ~10-fold difference in reporter levels was observed between minimal and maximal levels of proteasome inhibition. Remarkably however, mRFP-PrP$_{40–231}$ aggregates did not stabilize the reporter at all, even at time points after transfection when stabilization of nontranslocated proteins was readily observed (Figure 10B). This finding suggests that, although certain aggregates can inhibit proteasome under at least some conditions (Bence *et al.*, 2001), inhibition is not required for their ability to stabilize nontranslocated proteins. This conclusion is consistent with the results in Figure 2, where washout of proteasome inhibitor led to resumption of degradation of a proteasome-dependent substrate even though unprocessed, nontranslocated PrP was stabilized. Taken together, these findings suggest that stabilization of nontranslocated proteins by aggregates is at least partially selective and may indicate disturbance of quality control pathways upstream of the proteasome.

CONCLUSIONS AND PERSPECTIVE

In this study, we have found that cytosolic aggregates are capable of perturbing the pathway(s) of cytosolic quality control that normally degrade nontranslocated secretory and membrane protein precursors. This population of polypeptides is normally never observed, and was long thought to be a minor and perhaps irrelevant species. In recent years, however, the efficiency of protein translocation into the ER (and presumably other organelles) is appreciated to be less than perfect (Kim *et al.*, 2002; Rane *et al.*, 2004; Levine *et al.*, 2005; Kang *et al.*, 2006). Even from a theoretical standpoint, the biochemical reactions that mediate successful and selective targeting of signal-containing proteins to their correct destinations cannot be 100% efficient. Given that roughly one-third of all cellular proteins need to be targeted to the secretory pathway, even 0.1% inefficiency would constitute a substantial and constant source of nontranslocated proteins, most of which require disposal. Direct measurements of translocation efficiency suggest considerably higher levels of failed translocation (Levine *et al.*, 2005), particularly under conditions of ER stress (Kang *et al.*, 2006; Orsi *et al.*, 2006), further emphasizing the importance of cytosolic quality-control pathways. Such pathways appear to culminate at the proteasome, the inhibition of which stabilizes nontranslocated PrP, nontranslocated CRFR1, as well as proteins pharmacologically inhibited in their translocation (Besemer *et al.*, 2005; Garrison *et al.*, 2005). Although this study does not provide insight into what these pathways are, it does reveal that their efficient function can be compromised by different types of cytosolic aggregates.

The specific quality control pathway(s) that are inhibited by aggregates remain to be determined, but it seems unlikely to be solely the proteasome. Indeed, lack of global inhibition of the Ub-proteasome system is seen in transgenic mice expressing mutant Htt, in which Ub conjugates nonetheless accumulate (Maynard *et al.*, 2009). Candidates for perturbation would include chaperones and/or factors of the Ub-proteasome system, both of which have been found associated with aggregates (Cummings *et al.*, 1998; Donaldson *et al.*, 2003; Kaganovich *et al.*, 2008; Olzscha *et al.*, 2011). For example, Hsp70, p97, Ub, proteasomes, and other general quality control factors are often recovered in aggregates biochemically or visualized to colocalize with aggregates by immunofluorescence (e.g., Ma and Lindquist, 2001). It is therefore possible that partial inhibition of multiple factors (Olzscha *et al.*,

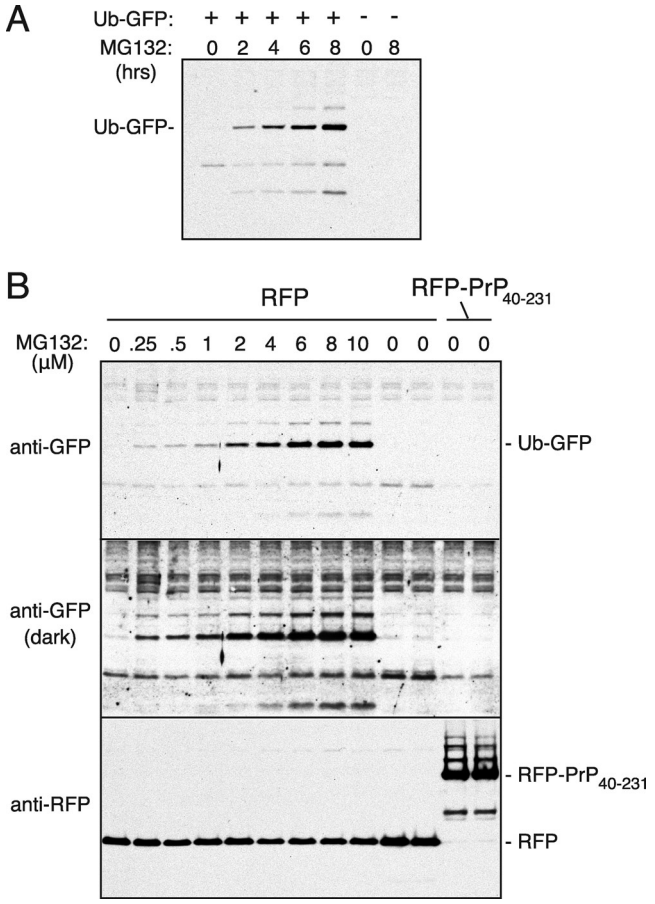

FIGURE 10: cyPrP aggregates do not detectably impair the proteasome. (A) Cells transfected with Ub-GFP were treated with 5 μM MG132 for various time periods and analyzed for GFP by immunoblotting. The primary Ub-GFP band is indicated. Note that minor bands above and below this major species probably represent ubiquitinated and degraded species, respectively. (B) Ub-GFP was cotransfected with either mRFP or mRFP-$PrP_{40–231}$. After 24 h, the cells were either left untreated or treated for 8 h with MG132 at the indicated concentrations. All cells were then harvested and analyzed by immunoblotting for GFP and RFP. Faint and dark exposures of the anti-GFP blot are shown. The MG132 titration illustrates that, even at low inhibitor concentrations, Ub-GFP stabilization is detectable. Coexpression of the mRFP-$PrP_{40–231}$ aggregates, however, shows no detectable Ub-GFP.

2011) leads to the net effect on nontranslocated proteins that we observe. Alternatively, specific proteins, such as a key Ub ligase or chaperone selective for nontranslocated precursors, might be inhibited by cytosolic aggregates. For now, answers to such questions must await delineation of the pathway(s) by which precursors are recognized and degraded, at which point key components can be tested.

Although not formally a precursor, a signal-deleted secretory pathway protein (carboxypeptidase Y) has been used as a model of cytosolic quality control in yeast. Thus far, degradation of this mislocalized protein has been shown to rely on chaperones (Park *et al.*, 2007) and the Ub ligases Ubr1, Ubr2, and San1 (Eisele and Wolf, 2008; Heck *et al.*, 2010; Nillegoda *et al.*, 2010). Parallel studies with an artificial "degron" showed that the ER-localized Doa10 Ub ligase represents yet another cytosolic quality control pathway in yeast (Ravid *et al.*, 2006; Metzger *et al.*, 2008). In multicellular eukaryotes, chaperones have also been implicated in cytosolic quality control via their interaction with the Ub ligase CHIP (McDonough and Patterson, 2003). It is unknown whether any of these pathways are directly involved in degrading nontranslocated precursors. Although it may seem obvious that the same pathways will be used by misfolded cytosolic proteins and nontranslocated precursors, it is worth noting that the latter are unique in having at least one highly hydrophobic domain. Indeed, our findings that a signal-containing precursor is differentially affected relative to a signal-cleaved version of the same protein (which is nonetheless mislocalized) suggest that different pathways are involved. Working out the upstream components of the cytosolic quality control pathway(s) for nontranslocated precursors therefore represents an important future goal.

Finally, it is worth considering whether our observations are potentially an artifact of overexpression. We do not believe this to be the case for several reasons. First, at least some of our studies with PrP were performed on stable cell lines the expression levels of which were similar to (or even lower than) those observed in normal brain. Second, earlier studies examining translocation efficiency of reporter proteins at a wide range of expression levels suggested that translocation inefficiency is not due to saturation but is an intrinsic property of some signal sequences (Rane *et al.*, 2004; Levine *et al.*, 2005). Third, even endogenous proteins may be reduced in their translocation during certain conditions, such as acute ER stress (Kang *et al.*, 2006). Fourth, in microscopy analyses, we observed similar effects in cells expressing different levels of the substrate protein. Thus it is likely that constant generation and degradation of precursors that have failed translocation is a basic cellular housekeeping process. Although we have surely exaggerated this phenomenon by overexpressing individual substrates to facilitate their analysis, there is good reason to believe that precursors are constantly fluxing through the cytosol en route to their proteasomal degradation.

Similarly, we believe that although we artificially generated aggregates by using specialized constructs or proteasome inhibition, our results may be relevant because it is increasingly clear that aggregates are a common feature of various disease states, and perhaps even normal aging (Cohen and Dillin, 2008; Morimoto, 2008). Furthermore, it has recently been appreciated that even extracellular aggregates are capable of accessing the cytosol by yet undetermined pathways (Clavaguera *et al.*, 2009; Desplats *et al.*, 2009; Frost *et al.*, 2009; Luk *et al.*, 2009; Ren *et al.*, 2009). Thus, although our observations are likely exaggerated in our model systems, we believe that they may hold relevance for protein misfolding disorders, including various neurodegenerative diseases. Indeed, perturbed quality control during aging and neurodegenerative disease is an emerging theme, and our findings now identify a new specific cytosolic quality control process that appears to be sensitive to perturbation by aggregates. It will now be important to understand this quality control pathway for nontranslocated proteins so that one can assess which step(s) are affected by aggregates and how this interference might contribute to the pathogenesis of protein-misfolding diseases.

MATERIALS AND METHODS

Constructs, antibodies, and reagents

A list of all constructs used in this study, their respective references, and a brief description of their characteristics is provided in Supplemental Table S1. PrP, Opn-PrP, and Prl-PrP encode hamster PrP with the signal sequences from either rat Opn or bovine Prl, and have been characterized previously (Rane *et al.*, 2004; Kang *et al.*, 2006). The mFP-tagged versions of these constructs and the mFP-$PrP_{40–231}$ constructs have been described (Chakrabarti and Hegde, 2009).

Human CRFR1 and Prl-CRFR1 in pCDNA-3.1 has been described (Kang *et al.*, 2006). Both constructs are tagged at the C terminus with an epitope (KTNMKHMAGAAA) recognized by the 3F4 antibody (from Signet Laboratories, Dedham, MA). PrP(SS+10)-GFP_{KDEL}, Prl(SS+10)-GFP_{KDEL}, PrP(10)-GFP_{KDEL}, and Prl(10)-GFP_{KDEL} all encode GFP with a C-terminal KDEL sequence in the pCDNA3.1 vector. The N terminus of these constructs contains either the first 32 residues of hamster PrP (22-residue signal sequence plus 10 mature residues), the first 40 residues of bovine Prl (30-residue signal sequence plus 10 mature residues), residues 23–32 of PrP, or residues 31–40 of Prl, respectively. All constructs contain an initiating methionine with optimal Kozak's consensus sequence. ΔSS-PrP and ΔSSΔGPI-PrP encode residues 23–254 and 23–231, respectively, of hamster PrP. Ub-GFP and GFP-Htt_{103} were gifts from N. Dantuma (Dantuma *et al.*, 2000) and L. Greene (Lee *et al.*, 2007). The mFP expression constructs were obtained from Clontech (Mountain View, CA). Antibodies were obtained from the following sources: 3F4 mouse monoclonal (Signet Laboratories); TRAPα (Fons *et al.*, 2003); GFP (Chakrabarti and Hegde, 2009); RFP (Chakrabarti and Hegde, 2009). MG132 was obtained from EMD Chemicals (Gibbstown, NJ).

Cell culture

N2a cells were cultured in DMEM containing 10% fetal bovine serum (FBS) at 5% CO2. Stable N2a cells expressing PrP or Opn-PrP have been described (Rane *et al.*, 2004; Kang *et al.*, 2006). Transient transfections were with Lipofectamine 2000 (Invitrogen, Carlsbad, CA). Biochemical assays using transient transfection were carried out 24 h posttransfection. Assays involving cell imaging were performed at time points as indicated in the figure legends. For live-cell confocal imaging experiments, cells were grown in 35-mm glass-bottom microwell dishes (MatTek, Ashland, MA), and those to be fixed and immunostained were grown in eight-well Lab-Tek chambered coverglass from Nunc/Thermo Fisher Scientific (Rochester, NY). For biochemical assays, cells grown in 6-, 12-, or 96-well tissue-culture dishes were used.

Biochemical analyses of cultured cells

Cells harvested for immunoblotting of total products were fully solubilized in 1% SDS, 0.1 M Tris, pH 8; boiled; vortexed vigorously to shear DNA; and analyzed by SDS–PAGE and blotting. These procedures permitted visualization of all species, instead of selecting the soluble species often observed when using other methods of lysis. Similarly, it is critical to fully solubilize and denature the whole cell in the pulse-chase studies to avoid selective visualization of only the soluble species. Pulse-chase analysis (Figure 2), deglycosylation (Figure 1A), and detergent solubility assays (Figure 3B) were as before (Rane *et al.*, 2004). The replating assay (Figures 1C and 3C) is described in the respective legends. Typically, cells in a six-well dish were treated with inhibitor as described, after which they were rinsed at least twice with phosphate-buffered saline (PBS). They were then trypsinized and replated into replicate wells of a 96-well dish to achieve ~70–90% density upon adherence. For the "0" time point, the cells were collected by centrifugation and solubilized in SDS. For the other time points (after the cells had adhered to the plate), the medium was removed and the adhered cells solubilized directly in SDS.

Fluorescence microscopy and imaging

Fluorescence microscopy was performed using a LSM510/ConfoCor 2 microscopy system (Zeiss, Thornwood, NY) equipped with an Ar-ion laser (for CFP or GFP excitation with the 458 nm and 488 nm lines, respectively) and a He-Ne laser (for RFP and Alexa-Fluor 594 excitation with the 543 line). A 40× or 63× 1.4 NA oil immersion objective was used for all imaging. For comparisons between multiple samples, images were collected during a single session by using identical excitation and detection settings. The detector gain settings were chosen to allow imaging of the desired cells within the linear range of the photomultiplier tube without saturating pixels. For imaging interactions between proteins, randomly chosen fields of cells were imaged at two detector gain settings to visualize both dim and bright cells. Three dishes were imaged for each set of transfections, and the complete set of experiments was performed thrice to eliminate artifacts arising from individual experiments. For FRAP analyses, a defined region of interest was photobleached at full laser power (100% power, 100% transmission); recovery of fluorescence was monitored by scanning the whole cell at low laser power (30% power, 0.3% transmission) as previously described (Snapp *et al.*, 2003). For immunofluorescence, transfected cells were stained as before (Rane *et al.*, 2004). In short, cells were fixed with 3.7% formaldehyde in PBS, rinsed with PBS, permeabilized and blocked for 1 h at room temperature in blocking buffer (PBS containing 10% FBS, 0.1% saponin, and 50 μg/ml RNase A), followed by incubation with diluted primary antibodies in blocking buffer for 1 h at room temperature. After washing, cells were incubated for 30 min with a 1:1000 (vol/vol) dilution of secondary antibody conjugated to Alexa-Fluor 594 (Invitrogen), washed with several changes of PBS (containing 10% FBS), and imaged in PBS (without FBS).

Quantification of imaging results

To quantify the experiments in Figures 5, 7, and 8, images of randomly selected fields (chosen without visualizing the test protein) were analyzed. Using ImageJ, the RGB-color images were split, and only the panel with expression profile of PrP, Prl-PrP, CRFR1, or Prl-CRFR1 (in the gray scale) was used for analysis. Cells coexpressing protein aggregates and the reporter proteins were identified manually, and only these were scored. The cells were demarcated into two areas representing the surface (perimeter) and intracellular regions, and the relative amount of fluorescence signal in each was measured. Any cell having more than 40% of the total signal arising from the intracellular population was considered "positive" for altered localization. Analysis for Figure 9 was done similarly, but using the z-stack image series to definitively identify the nucleus. Here cells where the GFP signal was diffusely nucleocytoplasmic throughout the z-stack were counted as altered; cells (by scanning the entire z-stack) that showed a clear demarcation between cytoplasm and nucleus, with reticular signal from the cytoplasm, were scored as normal. Approximately 50 cells were analyzed for this experiment. For Figure 4, coaggregation was judged to be positive if the test protein fluorescence was enriched in the aggregate or rimmed the surface of the aggregate. Approximately 200 cells were analyzed for this experiment.

ACKNOWLEDGMENTS

We thank Sang-Wook Kang for providing constructs, George Patterson and the Lippincott-Schwartz lab for microscopy support, Hegde lab members for constructive advice, and N. Dantuma and L. Greene for reagents.

REFERENCES

Aguzzi A, Rajendran L (2009). The transcellular spread of cytosolic amyloids, prions, and prionoids. Neuron 64, 783–790.

Alves-Rodrigues A, Gregori L, Figueiredo-Pereira ME (1998). Ubiquitin, cellular inclusions and their role in neurodegeneration. Trends Neurosci 21, 516–520.
Ashok A, Hegde RS (2008). Retrotranslocation of prion proteins from the endoplasmic reticulum by preventing GPI signal transamidation. Mol Biol Cell 19, 3463–3476.
Balch WE, Morimoto RI, Dillin A, Kelly JW (2008). Adapting proteostasis for disease intervention. Science 319, 916–919.
Ben-Zvi A, Miller EA, Morimoto RI (2009). Collapse of proteostasis represents an early molecular event in Caenorhabditis elegans aging. Proc Natl Acad Sci USA 106, 14914–14919.
Bence NF, Sampat RM, Kopito RR (2001). Impairment of the ubiquitin-proteasome system by protein aggregation. Science 292, 1552–1555.
Bennett EJ, Bence NF, Jayakumar R, Kopito RR (2005). Global impairment of the ubiquitin-proteasome system by nuclear or cytoplasmic protein aggregates precedes inclusion body formation. Mol Cell 17, 351–365.
Bennett EJ, Shaler TA, Woodman B, Ryu KY, Zaitseva TS, Becker CH, Bates GP, Schulman H, Kopito RR (2007). Global changes to the ubiquitin system in Huntington's disease. Nature 448, 704–708.
Besemer J, Harant H, Wang S, Oberhauser B, Marquardt K, Foster CA, Schreiner EP, de Vries JE, Dascher-Nadel C, Lindley IJ (2005). Selective inhibition of cotranslational translocation of vascular cell adhesion molecule 1. Nature 436, 290–293.
Chakrabarti O, Hegde RS (2009). Functional depletion of mahogunin by cytosolically exposed prion protein contributes to neurodegeneration. Cell 137, 1136–1147.
Clavaguera F *et al.* (2009). Transmission and spreading of tauopathy in transgenic mouse brain. Nat Cell Biol 11, 909–913.
Cohen E, Bieschke J, Perciavalle RM, Kelly JW, Dillin A (2006). Opposing activities protect against age-onset proteotoxicity. Science 313, 1604–1610.
Cohen E, Dillin A (2008). The insulin paradox: aging, proteotoxicity and neurodegeneration. Nat Rev Neurosci 9, 759–767.
Cummings CJ, Mancini MA, Antalffy B, DeFranco DB, Orr HT, Zoghbi HY (1998). Chaperone suppression of aggregation and altered subcellular proteasome localization imply protein misfolding in SCA1. Nat Genet 19, 148–154.
Dantuma NP, Lindsten K, Glas R, Jellne M, Masucci MG (2000). Short-lived green fluorescent proteins for quantifying ubiquitin/proteasome-dependent proteolysis in living cells. Nat Biotechnol 18, 538–543.
Desplats P, Lee HJ, Bae EJ, Patrick C, Rockenstein E, Crews L, Spencer B, Masliah E, Lee SJ (2009). Inclusion formation and neuronal cell death through neuron-to-neuron transmission of alpha-synuclein. Proc Natl Acad Sci USA 106, 13010–13015.
DiFiglia M, Sapp E, Chase KO, Davies SW, Bates GP, Vonsattel JP, Aronin N (1997). Aggregation of huntingtin in neuronal intranuclear inclusions and dystrophic neurites in brain. Science 277, 1990–1993.
Donaldson KM, Li W, Ching KA, Batalov S, Tsai CC, Joazeiro CA (2003). Ubiquitin-mediated sequestration of normal cellular proteins into polyglutamine aggregates. Proc Natl Acad Sci USA 100, 8892–8897.
Drisaldi B, Stewart RS, Adles C, Stewart LR, Quaglio E, Biasini E, Fioriti L, Chiesa R, Harris DA (2003). Mutant PrP is delayed in its exit from the endoplasmic reticulum, but neither wild-type nor mutant PrP undergoes retrotranslocation prior to proteasomal degradation. J Biol Chem 278, 21732–21743.
Duennwald ML, Lindquist S (2008). Impaired ERAD and ER stress are early and specific events in polyglutamine toxicity. Genes Dev 22, 3308–3319.
Eisele F, Wolf DH (2008). Degradation of misfolded protein in the cytoplasm is mediated by the ubiquitin ligase Ubr1. FEBS Lett 582, 4143–4146.
Fons RD, Bogert BA, Hegde RS (2003). Substrate-specific function of the translocon-associated protein complex during translocation across the ER membrane. J Cell Biol 160, 529–539.
Frost B, Ollesch J, Wille H, Diamond MI (2009). Conformational diversity of wild-type Tau fibrils specified by templated conformation change. J Biol Chem 284, 3546–3551.
Garrison JL, Kunkel EJ, Hegde RS, Taunton J (2005). A substrate-specific inhibitor of protein translocation into the endoplasmic reticulum. Nature 436, 285–289.
Gidalevitz T, Ben-Zvi A, Ho KH, Brignull HR, Morimoto RI (2006). Progressive disruption of cellular protein folding in models of polyglutamine diseases. Science 311, 1471–1474.
Heck JW, Cheung SK, Hampton RY (2010). Cytoplasmic protein quality control degradation mediated by parallel actions of the E3 ubiquitin ligases Ubr1 and San1. Proc Natl Acad Sci USA 107, 1106–1111.
Huang CC, Faber PW, Persichetti F, Mittal V, Vonsattel JP, MacDonald ME, Gusella JF (1998). Amyloid formation by mutant huntingtin: threshold, progressivity and recruitment of normal polyglutamine proteins. Somat Cell Mol Genet 24, 217–233.
Kaganovich D, Kopito R, Frydman J (2008). Misfolded proteins partition between two distinct quality control compartments. Nature 454, 1088–1095.
Kang SW, Rane NS, Kim SJ, Garrison JL, Taunton J, Hegde RS (2006). Substrate-specific translocational attenuation during ER stress defines a preemptive quality control pathway. Cell 127, 999–1013.
Kim SJ, Mitra D, Salerno JR, Hegde RS (2002). Signal sequences control gating of the protein translocation channel in a substrate-specific manner. Dev Cell 2, 207–217.
Kopito RR (2000). Aggresomes, inclusion bodies and protein aggregation. Trends Cell Biol 10, 524–530.
Lee KJ, Panzera A, Rogawski D, Greene LE, Eisenberg E (2007). Cellular prion protein (PrPC) protects neuronal cells from the effect of huntingtin aggregation. J Cell Sci 120, 2663–2671.
Levine CG, Mitra D, Sharma A, Smith CL, Hegde RS (2005). The efficiency of protein compartmentalization into the secretory pathway. Mol Biol Cell 16, 279–291.
Li W, Tu D, Brunger AT, Ye Y (2007). A ubiquitin ligase transfers preformed polyubiquitin chains from a conjugating enzyme to a substrate. Nature 446, 333–337.
Lowe J, Blanchard A, Morrell K, Lennox G, Reynolds L, Billett M, Landon M, Mayer RJ (1988). Ubiquitin is a common factor in intermediate filament inclusion bodies of diverse type in man, including those of Parkinson's disease, Pick's disease, and Alzheimer's disease, as well as Rosenthal fibres in cerebellar astrocytomas, cytoplasmic bodies in muscle, and mallory bodies in alcoholic liver disease. J Pathol 155, 9–15.
Luk KC, Song C, O'Brien P, Stieber A, Branch JR, Brunden KR, Trojanowski JQ, Lee VM (2009). Exogenous alpha-synuclein fibrils seed the formation of Lewy body-like intracellular inclusions in cultured cells. Proc Natl Acad Sci USA 106, 20051–20056.
Ma J, Lindquist S (2001). Wild-type PrP and a mutant associated with prion disease are subject to retrograde transport and proteasome degradation. Proc Natl Acad Sci USA 98, 14955–14960.
Ma J, Lindquist S (2002). Conversion of PrP to a self-perpetuating PrPSc-like conformation in the cytosol. Science 298, 1785–1788.
Maynard CJ *et al.* (2009). Accumulation of ubiquitin conjugates in a polyglutamine disease model occurs without global ubiquitin/proteasome system impairment. Proc Natl Acad Sci USA 106, 13986–13991.
McDonough H, Patterson C (2003). CHIP: a link between the chaperone and proteasome systems. Cell Stress Chaperones 8, 303–308.
Metzger MB, Maurer MJ, Dancy BM, Michaelis S (2008). Degradation of a cytosolic protein requires endoplasmic reticulum-associated degradation machinery. J Biol Chem 283, 32302–32316.
Morimoto RI (2008). Proteotoxic stress and inducible chaperone networks in neurodegenerative disease and aging. Genes Dev 22, 1427–1438.
Nillegoda NB, Theodoraki MA, Mandal AK, Mayo KJ, Ren HY, Sultana R, Wu K, Johnson J, Cyr DM, Caplan AJ (2010). Ubr1 and ubr2 function in a quality control pathway for degradation of unfolded cytosolic proteins. Mol Biol Cell 21, 2102–2116.
Norstrom EM, Ciaccio MF, Rassbach B, Wollmann R, Mastrianni JA (2007). Cytosolic prion protein toxicity is independent of cellular prion protein expression and prion propagation. J Virol 81, 2831–2837.
Nucifora FC Jr *et al.* (2001). Interference by huntingtin and atrophin-1 with cbp-mediated transcription leading to cellular toxicity. Science 291, 2423–2428.
Olzscha H, Schermann SM, Woerner AC, Pinkert S, Hecht MH, Tartaglia GG, Vendruscolo M, Hayer-Hartl M, Hartl FU, Vabulas RM (2011). Amyloid-like aggregates sequester numerous metastable proteins with essential cellular functions. Cell 144, 67–78.
Orsi A, Fioriti L, Chiesa R, Sitia R (2006). Conditions of endoplasmic reticulum stress favor the accumulation of cytosolic prion protein. J Biol Chem 281, 30431–30438.
Park SH, Bolender N, Eisele F, Kostova Z, Takeuchi J, Coffino P, Wolf DH (2007). The cytoplasmic Hsp70 chaperone machinery subjects misfolded and endoplasmic reticulum import-incompetent proteins to degradation via the ubiquitin-proteasome system. Mol Biol Cell 18, 153–165.
Rane NS, Chakrabarti O, Feigenbaum L, Hegde RS (2010). Signal sequence insufficiency contributes to neurodegeneration caused by transmembrane prion protein. J Cell Biol 188, 515–526.

Rane NS, Kang SW, Chakrabarti O, Feigenbaum L, Hegde RS (2008). Reduced translocation of nascent prion protein during ER stress contributes to neurodegeneration. Dev Cell 15, 359–370.
Rane NS, Yonkovich JL, Hegde RS (2004). Protection from cytosolic prion protein toxicity by modulation of protein translocation. EMBO J 23, 4550–4559.
Ravid T, Kreft SG, Hochstrasser M (2006). Membrane and soluble substrates of the Doa10 ubiquitin ligase are degraded by distinct pathways. EMBO J 25, 533–543.
Ravikumar B *et al*. (2004). Inhibition of mTOR induces autophagy and reduces toxicity of polyglutamine expansions in fly and mouse models of Huntington disease. Nat Genet 36, 585–595.
Ren PH, Lauckner JE, Kachirskaia I, Heuser JE, Melki R, Kopito RR (2009). Cytoplasmic penetration and persistent infection of mammalian cells by polyglutamine aggregates. Nat Cell Biol 11, 219–225.
Robinson P, Lebel M, Cyr M (2008). Dopamine D1 receptor-mediated aggregation of N-terminal fragments of mutant huntingtin and cell death in a neuroblastoma cell line. Neuroscience 153, 762–772.
Ross CA, Pickart CM (2004). The ubiquitin-proteasome pathway in Parkinson's disease and other neurodegenerative diseases. Trends Cell Biol 14, 703–711.
Rubinsztein DC (2006). The roles of intracellular protein-degradation pathways in neurodegeneration. Nature 443, 780–786.
Satyal SH, Schmidt E, Kitagawa K, Sondheimer N, Lindquist S, Kramer JM, Morimoto RI (2000). Polyglutamine aggregates alter protein folding homeostasis in Caenorhabditis elegans. Proc Natl Acad Sci USA 97, 5750–5755.
Schaffar G, Breuer P, Boteva R, Behrends C, Tzvetkov N, Strippel N, Sakahira H, Siegers K, Hayer-Hartl M, Hartl FU (2004). Cellular toxicity of polyglutamine expansion proteins: mechanism of transcription factor deactivation. Mol Cell 15, 95–105.
Selkoe DJ (2003). Folding proteins in fatal ways. Nature 426, 900–904.
Snapp EL, Hegde RS, Francolini M, Lombardo F, Colombo S, Pedrazzini E, Borgese N, Lippincott-Schwartz J (2003). Formation of stacked ER cisternae by low affinity protein interactions. J Cell Biol 163, 257–269.
Soto C, Estrada L, Castilla J (2006). Amyloids, prions and the inherent infectious nature of misfolded protein aggregates. Trends Biochem Sci 31, 150–155.
Trojanowski JQ, Lee VM (2000). "Fatal attractions" of proteins. A comprehensive hypothetical mechanism underlying Alzheimer's disease and other neurodegenerative disorders. Ann NY Acad Sci 924, 62–67.
Willingham S, Outeiro TF, DeVit MJ, Lindquist SL, Muchowski PJ (2003). Yeast genes that enhance the toxicity of a mutant huntingtin fragment or alpha-synuclein. Science 302, 1769–1772.
Zhang F, Strom AL, Fukada K, Lee S, Hayward LJ, Zhu H (2007). Interaction between familial amyotrophic lateral sclerosis (ALS)-linked SOD1 mutants and the dynein complex. J Biol Chem 282, 16691–16699.

Supplementary Materials for:

Cytosolic aggregates perturb the degradation of non-translocated secretory and membrane proteins

Oishee Chakrabarti [1,2,*], Neena S. Rane[1], and Ramanujan S. Hegde[1,*]

[1]Cell Biology and Metabolism Program
Eunice Kennedy Shriver National Institute
of Child Health and Human Development
National Institutes of Health
18 Library Drive, Bldg. 18, Room 101
Bethesda, MD, 20892, USA

[2]Current address:
Saha Institute of Nuclear Physics
Sector-1, Block-AF, Room 4622
Bidhannagar
Kolkata-700 064, India

*Correspondence: oishee.chakrabarti@saha.ac.in or hegder@mail.nih.gov

Supplementary Table S1 – Description of constructs used in this study. Note that mFP refers to monomeric fluorescent protein. The specific FPs are indicated in the text (e.g., GFP, RFP and CFP refer to green, red and cyan fluorescent proteins, respectively).

Name	Description	Localization	Biochemical Properties	Reference
PrP	Wild type Syrian hamster sequence	Plasma membrane, secretory pathway, endocytic pathway, cytosol (~10%)	Major population is soluble, glycosylated, and GPI anchored. Minor cytosolic population is rapidly degraded by the proteasome and normally not observed at steady-state.	Rane et al., 2004
Opn-PrP	Signal of PrP (residues 1-22) replaced with signal from rat osteopontin	Same as PrP, but without an appreciable cytosolic population.	Same as major population of PrP.	Rane et al., 2004
Prl-PrP	Signal of PrP replaced with signal from bovine prolactin	Same as Opn-PrP, but without an appreciable cytosolic population.	Same as major population of PrP	Rane et al., 2004
ΔSS-PrP	Deletion of residues 2-22 of PrP.	Cytosolic	Rapidly degraded by proteasome. Insoluble upon stabilization with proteasome inhibitors.	Rane et al., 2008 Ashok and Hegde, 2008
ΔSSΔGPI-PrP	Deletion of residues 2-22 and 232-254.	Cytosolic	Rapidly degraded by proteasome. Insoluble upon stabilization with proteasome inhibitors.	Ashok and Hegde, 2008
PrP-mFP	FP inserted into PrP at codon 51.	Same as PrP	Same as PrP.	Rane et al., 2004 Chakrabarti and Hegde 2009
Opn-PrP-mFP	Same as PrP-mFP but with signal from Opn.	Same as Opn-PrP	Same as Opn-PrP	Rane et al., 2004
Prl-PrP-mFP	Same as PrP-mFP but with signal from Prl.	Same as Prl-PrP	Same as Prl-PrP	This study
mFP-PrP_{40-231}	mFP followed by residues 40-231 of PrP	Cytosolic in discrete puncta.	Highly aggregation prone and poorly degraded by the proteasome.	Chakrabarti and Hegde, 2009
CRFR1-3F4	Human CRFR1 tagged at C-terminus with 3F4 epitope.	Plasma membrane, secretory pathway, endocytic pathway, cytosol (~10%)	Major population is 7-TM glycoprotein. Minor cytosolic population is rapidly degraded by the proteasome and normally not observed at steady-state.	Kang et al., 2006
Prl-CRFR1-3F4	Same as CRFR1 but containing the Prl signal sequence.	Same as CRFR1 but with less of the cytosolic population.	Same as CRFR1.	Kang et al., 2006
PrP(SS+10)-mFP_{KDEL}	First 32 residues of PrP (signal plus ten mature domain residues) followed by mFP and a KDEL sequence.	ER lumen (~90%) and minor cytosolic pool (~10%)	Soluble. Minor cytosolic population degraded by proteasome, and remains soluble upon stabilization.	This study
Prl(SS+10)-mFP_{KDEL}	First 40 residues of Prl (signal plus ten mature domain residues) followed by mFP and a KDEL sequence.	ER lumen with very minor cytosolic pool (<2%).	Soluble. Minor cytosolic population degraded by proteasome, and remains soluble upon stabilization.	This study
PrP(10)-mFP_{KDEL}	Residues 23-32 of PrP followed by mFP and a KDEL sequence.	Cytosolic	Soluble at steady-state.	This study
Prl(10)-mFP_{KDEL}	Residues 31-40 of Prl followed by mFP and a KDEL sequence.	Cytosolic	Soluble at steady-state.	This study
FP-HttQ103	mFP fused to Exon 1 of Htt containing 103 glutamines.	Cytosolic; some cells show puncta, others are diffuse.	Aggregation-prone and poorly degraded by the proteasome.	Lee et al., 2007 Chakrabarti and Hegde, 2009
Ub-GFP	Ubiquitin G76V fused to GFP	Cytosolic	Rapidly degraded by the proteasome; is diffusely cytosolic when stabilized.	Dantuma et al., 2000

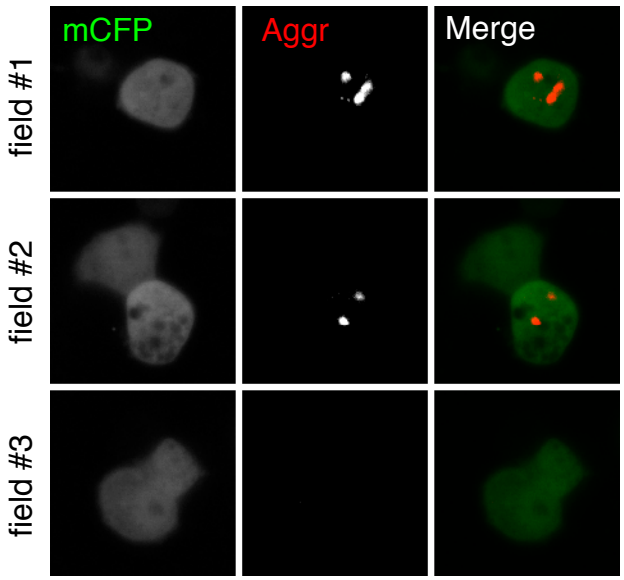

Sup. Fig. S1. CFP does not co-aggregate with cytosolic PrP aggregates. Monomeric CFP (mCFP) was co-transfected with RFP-PrP_{40-231} and analyzed as in Fig. 4. The mCFP is shown in the green channel, and the PrP aggregates shown in the red channel. Three examples are shown. Fields 1 and 2 show cells that contain aggregates, while field 3 shows a cell lacking aggregates. Note that mCFP remains distributed uniformly through the nucleocytoplasmic compartment in the presence or absence of aggregates, with no visible enrichment or rimming around the aggregate. Similar results were seen with other FPs (not shown).

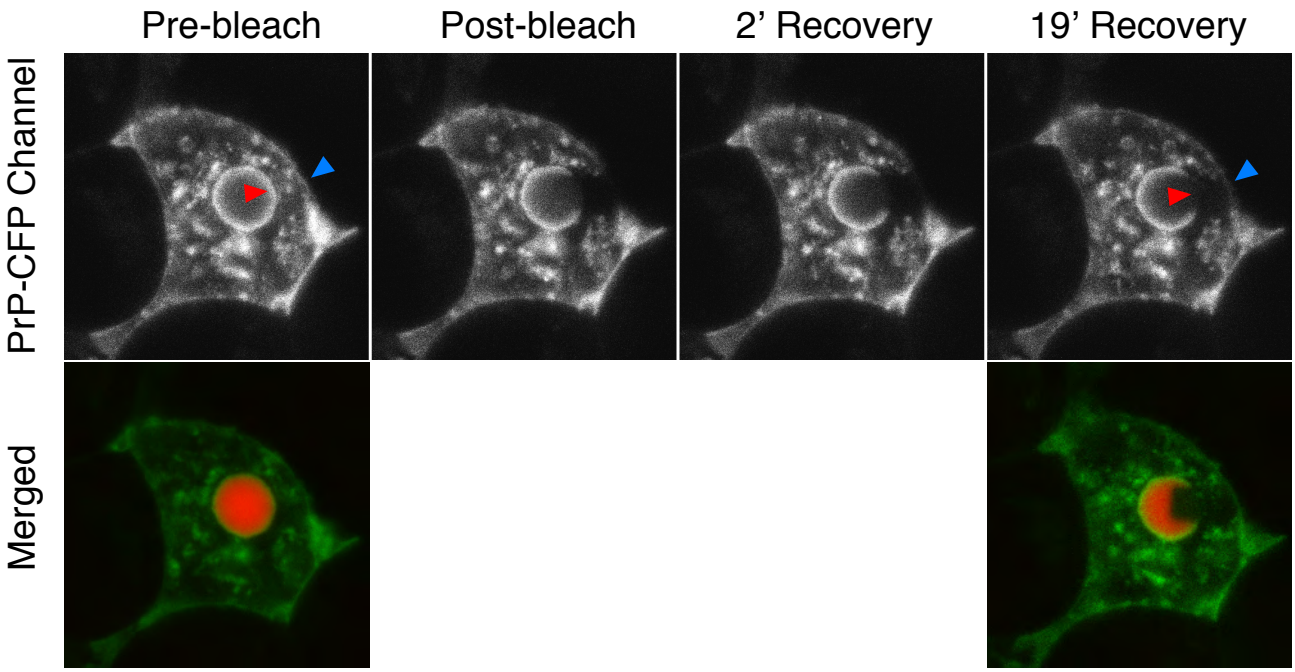

Sup. Fig. S2. Co-aggregated PrP is diffusionally immobile. An aggregate-containing cell co-expressing PrP-CFP and RFP-PrP_{40-231} was analyzed by FRAP as in Fig. 4C. A region containing approximately half of an apparent aggregate (red arrowhead) as well as a section of the plasma membrane (blue arrowhead) was photobleached (in both the CFP and RFP channels), and monitored for 20 min at 1 min intervals. Shown are the images immediately before and after the photobleaching, as well as after 2 and 19 min of recovery. Note that the thin rim of PrP-CFP fluorescence at the plasma membrane has recovered in the 19 min image (blue arrowhead), but the protein on the surface of the aggregate (red arrowhead) remains bleached even at 19 min. Upper images show the PrP-CFP channel, and the lower images show the merged channel illustrating that the mRFP-PrP_{40-231} (red) shows no recovery 19 min after photobleaching.

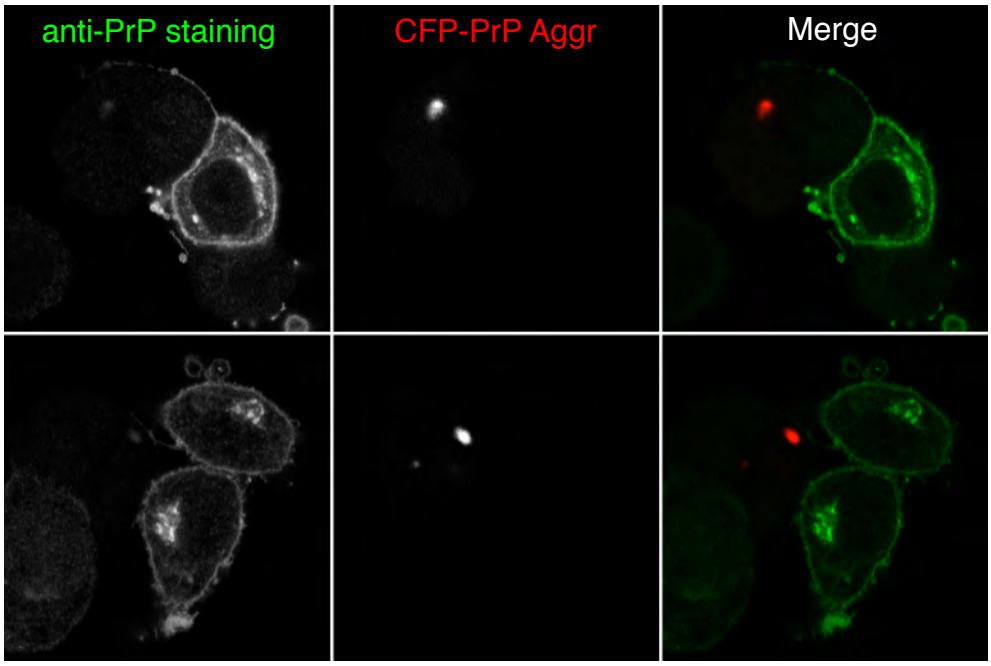

Sup. Fig. S3. PrP aggregates stain poorly with anti-PrP antibodies. N2a cells were transfected with CFP-PrP_{40-231} to generate PrP aggregates in the cytosol. A separate set of N2a cells were transfected with wild type PrP. After transfection, the two sets of cells were mixed together and replated onto coverslips. 18 h later, they were fixed and processed for immunofluorescence using 3F4 anti-PrP antibodies. The CFP fluorescence, the immunofluorescent signal, and the merged image are shown for two fields. Note that the PrP aggregate stains poorly with the 3F4 antibody, while the non-aggregated PrP in the secretory pathway and cell surface serves as a positive control for staining. Similar results were obtained for a different anti-PrP antibody (data not shown).

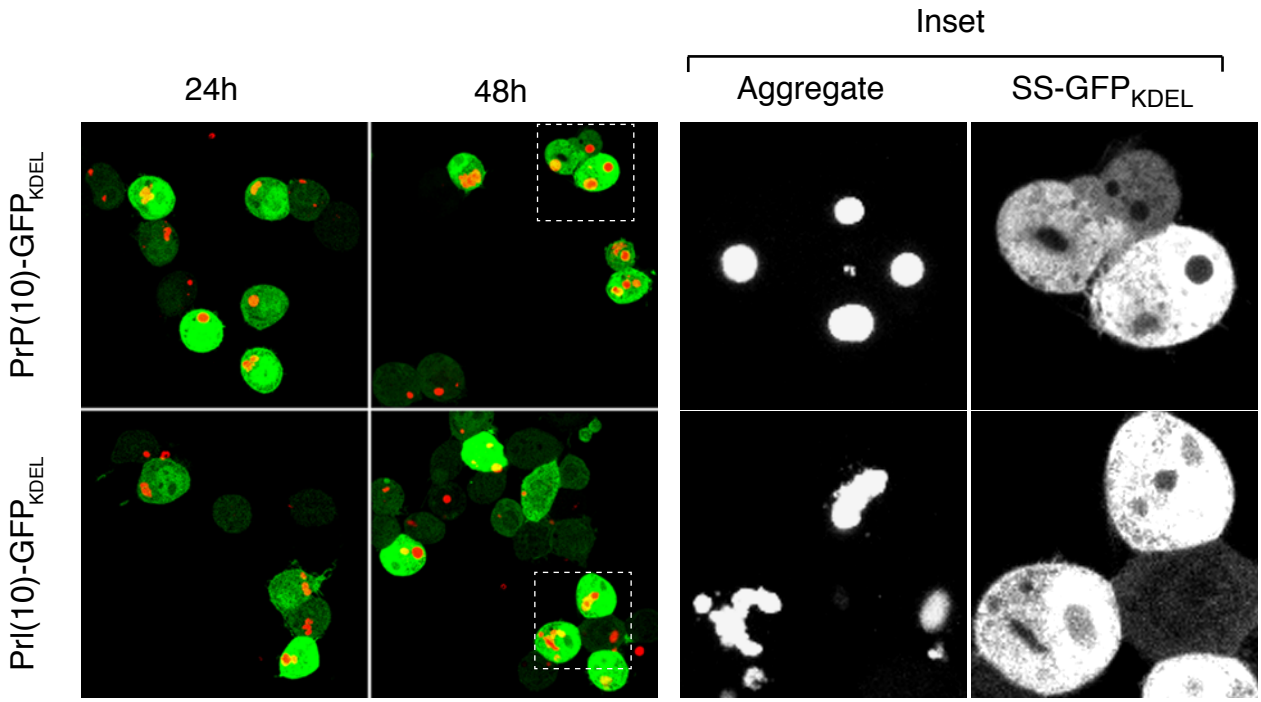

Sup. Fig. S4. Cytosolic GFP is unaffected by PrP aggregates. N2a cells were co-transfected with the indicated GFP constructs and RFP-PrP$_{40-231}$ to generate PrP aggregates in the cytosol. The GFP constructs contain the first ten residues of the mature domain of either PrP or Prl fused to the N-terminus, and the KDEL sequence fused to the C-terminus. They are identical to the constructs in Fig. 9, except lacking the signal sequence, and are therefore localized in the cytosol. The transfected cells were imaged at 24 and 48 hrs. The region marked by the white box was enlarged and shown as split images to illustrate that the GFP does not show evidence of co-aggregation with the RFP-PrP aggregates (i.e., it remains diffusely localized, without any obvious enrichment or rimming around the aggregate. Instead, the GFP is often excluded from the aggregate regions.